

The Genesis of Nano-Micron-Sized Spheroidal Aggregates of FeS₂ in the Laozuoshan Gold Deposit, Heilongjiang Province, NE China

Lin Meng¹, Fei Huang^{1,*}, Jia Liu², Miaomiao Xing¹, Quan Wan³, Jiaqi Ling¹,
Shang Gao¹, and Wenyuan Gao¹

¹Key Laboratory of Ministry of Education on Safe Mining of Deep Metal Mines and School of Resources and Civil Engineering, Northeastern University, Shenyang 110819, China

²Gemmological Institute, China University of Geosciences (Wuhan), Wuhan 430074, China

³State Key Laboratory of Ore Deposit Geochemistry, Institute of Geochemistry Chinese Academy of Sciences, Guiyang 550081, China

Nano-micron-sized spheroidal aggregates of FeS₂ has been found from the Laozuoshan gold deposit, Heilongjiang Province, NE China. There are diversified morphology, some as large or small girdles, and some as paragenesis of aggregates through cementation. Most of such aggregates distribute at the edge of pyrrhotite before metasomatized by arsenopyrite. Through a systematic observation on the micro-structure, grain size and components of nano-micron-sized spheroidal aggregates of FeS₂ by means of Field Emission Scanning Electron Microscopy (FE-SEM), Electron Probe Micro Analysis (EPMA) and *in situ* micro X-ray Diffraction (XRD), etc. We found such aggregates are composed of nano-micron-sized grains gathered together, part of which have an euhedral structure, with a crystalline grain size of 50 nm–<1 μm. The aggregates of FeS₂ are composed of pyrite and marcasite, and the crystal face diffraction peak intensities of pyrite (200) and (311) decline remarkably from the center to the edge, and the crystal face diffraction peak intensities of marcasite (110) and (311) in the center are lower than those at the edge. From the center to the edge, the content of Fe in nano-micron-sized spheroidal aggregates changes slightly, but the S content declines remarkably at the edge, and the content of As is low in the center but grows remarkably at the edge. In addition, there are low-temperature minerals such as chalcedony and carbonates (like calcite) filled along the edge of or in the fissures among spheroidal aggregates of FeS₂. Based on the above study in combination of the fluid inclusion characteristics of the mineral deposit, we suggest that the spheroidal aggregates of FeS₂ are formed under the drive of free energy on the surface of nano-sized FeS₂ crystals, which nucleates rapidly in a static fluid environment due to fluid getting supersaturated. The spheroidal aggregates of FeS₂ indicate that under low temperature conditions, the pH value of fluid changes from medium acidity to acidity throughout the crystallization process.

Keywords: Laozuoshan Gold Deposit, Spheroidal Aggregates of FeS₂, Pyrite, Marcasite, Genetic Mineralogy.

1. INTRODUCTION

Pyrite and marcasite are two polymorphisms of FeS₂. The micro-morphology and chemical components of pyrite are of significance for revealing the geological environment and mineralization medium of FeS₂, as well

as the genesis of mineral deposit.^{1–4} It is generally agreed that marcasite, as a low temperature phase of FeS₂, takes shape under the conditions of pH < 5 and T < 240 °C.⁵ It is also discovered in the study that sulfur species (e.g., polysulfides, polythionates or thiosulfates), if any, are favorable for the formation of pyrite and marcasite.^{6,7}

*Author to whom correspondence should be addressed.

Pyrite is widely distributed with diversified morphology, of which pyrite in mono-crystal structure is more common than the framboidal growth of pyrite crystals of similar size and shape.^{8–14}

It is also discovered in previous research by others that pyrite may exhibit a colloidal growth,^{15,16} whose genesis is mainly as below:

- (1) coagulation and precipitation of colloidal solution;¹⁷
- (2) chemical crystallization of solution due to super-saturation,^{15,16,18–26}
- (3) Biochemical sedimentation.^{27,28}

A great deal of research achievements indicate that colloidal pyrite records the changes in the physicochemical conditions of ore-bearing hydrothermal solutions throughout the ore-forming process,^{29–33} and accordingly, the physicochemical conditions of the geological environment can be identified.^{16,19,23,34}

The spheroidal aggregates of FeS₂ discovered at the east ore belt of the Laozuoshan gold deposit, Heilongjiang province, China by the writers are composed of pyrite and marcasite, but have indifferent characteristics as compared with framboidal and colloidal pyrite.

The data about the components and *in situ* micro-XRD of nano-micron-sized spheroidal aggregates of FeS₂ are obtained after a systematic observation is carried out on their morphology, structural characteristics and the law on paragenetic assemblage. In this paper, the genesis of nano-micron-sized spheroidal aggregates of FeS₂ is analyzed and discussed, with a view to revealing the physicochemical environment and hydrothermal process during their formation.

2. REGIONAL GEOLOGY

The Laozuoshan gold deposit is located on the Jiamusi uplift of the Ji-Hei fold system. The exposure strata inside the mining area include Lower Proterozoic Mashan group, Chengzihe formation of Mesozoic Jurassic system and Quaternary unconsolidated sediments as arranged from old to new. What exposures from the Mashan group are quartz-mica schist, amphibolite gneiss, graphite schist, biotite plagiogneiss, marble and hybrid rock, etc., of which the marble and hybrid rock exposure in large area are the main ore-bearing horizon of the Laozuoshan gold deposit. Sand rock and carbonaceous shale exposed from the Chengzihe formation intersect in an unconformable way with Hercynian gneissic granite, as shown in Figure 1.³⁵

The fault structure of this mining area develops extremely, characterized by its complexity and multiple-stage growth, which is mainly along two directions, that is, NW and NE, while the fault along the NW direction takes control of the formation of the Laozuoshan gold deposit. Magmatic rock is widely distributed over the mining area, mainly including Xingdong granite and Hercynian granite formed in the early Proterozoic era, while Yanshanian medium-acid magmatic has sparse exposure.

Consisting of three ore belts from west to east, the Laozuoshan gold deposit experienced the mid and late Hercynian tectonic-magmatic events (264–281 Ma) and the Yanshanian neutral-acid magmatic events (105–146 Ma).³⁶ In the early stage, this mineral deposit experienced magmatic-tectonic events in the mid and late Hercynian age before skarn gold deposit was formed from the Mashan group marble inside the mineral-contained

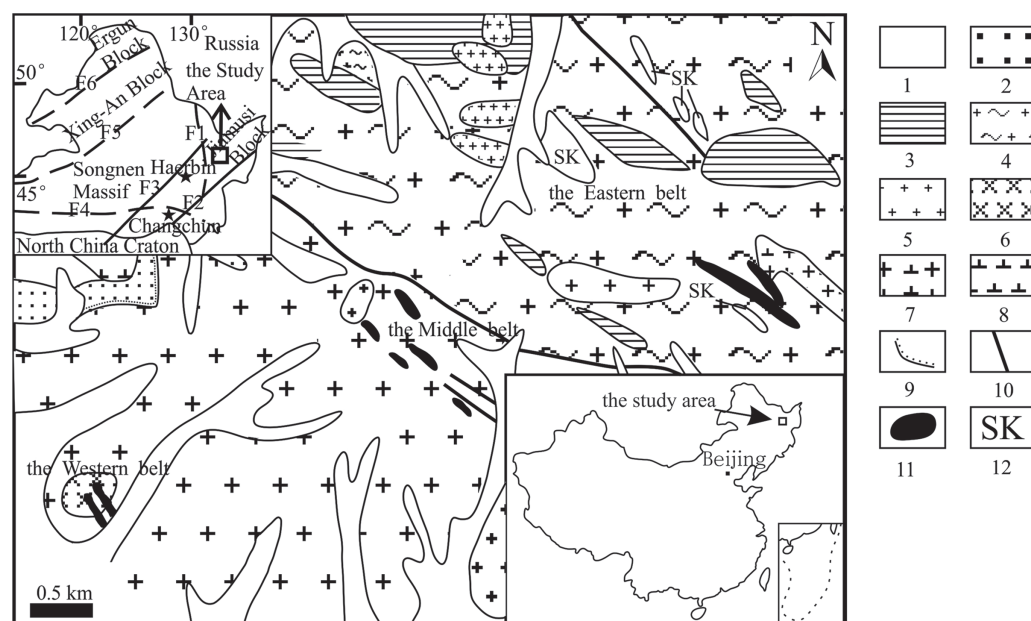


Figure 1. Geologic map of the Laozuoshan mining area. 1—Quaternary; 2—Jurassic; 3—Lower Proterozoic Mashan group; 4—Xingdong granite; 5—Hercynian granite; 6—Yanshanian magmatic; 7—Granodiorite; 8—Diorite porphyrite; 9—Unconformable boundary; 10—Fault; 11—Orebody; 12—Skarn; F1: Mudanjiang fault; F2: Dunhua-Mishan fault; F3: Yitong-Yilan fault; F4: Xilamulun River-Changchun fault; F5: Nenjiang fault; F6: Tayuan-Xiguitu fault.

hydrothermal metasomatism area. The skarn mineralization can be classified into three stages, that is, pyrrhotite + arsenopyrite ± quartz (I); colloidal pyrite + marcasite + chalcedony (II); coarse arsenopyrite + calcite + quartz (III). The east and middle ore belts were mainly formed at this mineralization stage. In the Yanshanian medium-acid magmatic events, magma hydrothermal fluids overlapped on the skarn orebody to make the orebody further concentrated.^{35,37,38} The hydrothermal action in this age can be classified into four stages, that is, the quartz stage (I), the coarse arsenopyrite + quartz + calcite stage (II), multi-metal sulfide stage (III), and calcite ± quartz (IV).³⁷

3. BASIC CHARACTERISTICS OF ORE

Samples are taken from the southeast section of the east ore belt. The orebody wall rocks are mainly composed of skarn, hybrid rock, silicified and carbonate rocks as well as tectonic breccia, with skarn constituting the main components of the orebody bastard.³⁹ Within the research area, the metal sulfides contained in the ore mainly include pyrrhotite, arsenopyrite, pyrite and chalcopyrite, followed by sphalerite and galena, etc., and the gangue minerals mainly include quartz, calcite, diopside, garnet, epidote

and sericite, etc. The minerals exit with a metasomatic texture, euhedral or subhedral grain structure and colloidal structure, etc. The ore structures mainly include disseminated structure and dense massive structure. There are a number of wall rock alterations, of which skarnization, silicification, chloritization and carbonation have the closest relationship with mineralization.

According to the relationship between structure and paragenetic assemblage, pyrite from the Laozuoshan gold deposit can be classified into four generations, marked with Py I, Py II, Py III and Py IV respectively (Fig. 2). Py I is euhedral and nearly equigranular, with a grain size of 20–36 μm, occasionally visible in the spheroidal aggregates of FeS₂ (Py II) (Fig. 2(a)). The colloidal Py II is distributed in the orebodies along tectonic contact zones of migmatitic granite and calcareous marble appearing as colloid crystals, on which there are concentric cones with different size ranging from 100 μm to 2 cm, and accompanied by the first-generation pyrrhotite (Po I) and the second-generation arsenopyrite (Apy II) (Fig. 2(b)); Py III exists in the tectonic zones of the Yanshanian neutral-acid hypabyssal rocks superposed above the skarn formed at earlier stages appearing mainly in an euhedral-subhedral granular texture {100} or {100} + {111} with a grain size of 300 μm–5 mm, and coexists with the second-generation

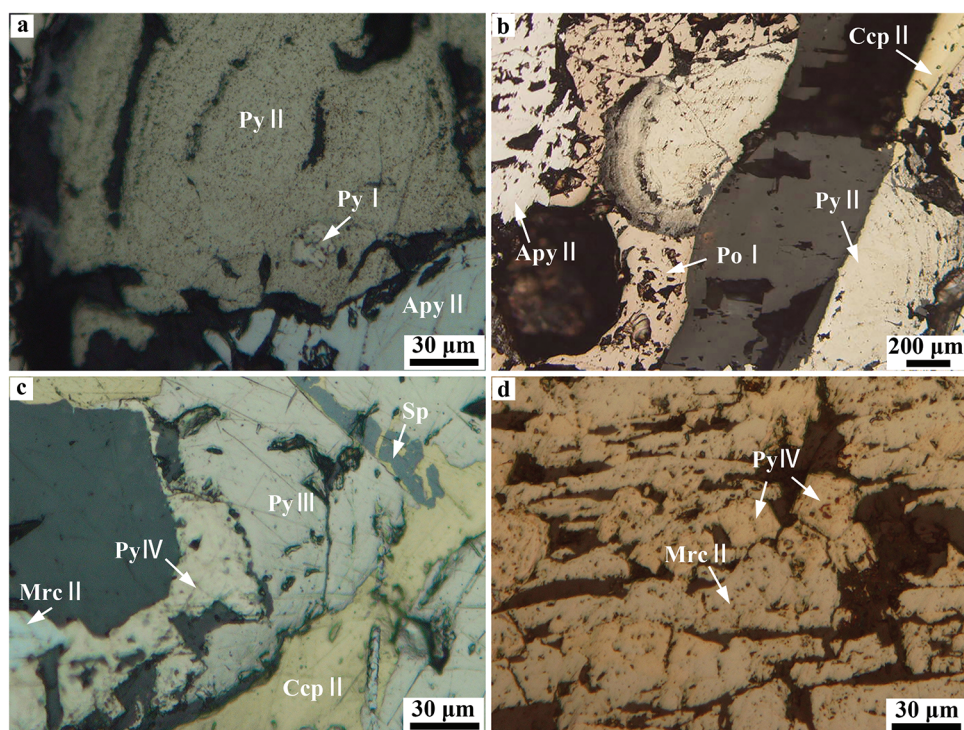


Figure 2. Characteristics of four generations of pyrite paragenetic minerals from Laozuoshan gold deposit. (a) Pyrite (Py I) is encapsulated by spheroidal aggregates of FeS₂ (Py II), which has been metasomatized by arsenopyrite (Apy II) at the edge; (b) Spheroidal aggregates of FeS₂ (Py II) are penetrated by later-formed hydrothermal fluid; (c) Coarse euhedral pyrite (Py III) is metasomatized by later-formed pyrite (Py IV) and pyrite (Py III) metasomatized by chalcopyrite (Ccp II) and sphalerite; (d) fine and euhedral pyrite (Py IV) is distributed between marcasite bands (Mrc II); Py I-first-generation pyrite; PyII-spheroidal aggregates of FeS₂; Py III-third-generation pyrite; Py IV-fourth-generation pyrite; Po I-first-generation pyrrhotite; Po II-second-generation pyrrhotite; Apy II-second-generation arsenopyrite; Ccp I-first-generation chalcopyrite; Ccp II-second-generation chalcopyrite; Sp-sphalerite.

chalcopyrite (Ccp II), the second-generation pyrrhotite (Po II), the third-generation arsenopyrite (Apy III) and the first-generation sphalerite (Sp I) (as shown in Fig. 2(c)); Py IV and Py III, as minerals formed at the early stage of metasomatism, are produced from the same place and coexists mainly with the second-generation marcasite (Mrc II), appearing mainly in an euhedral-subhedral granular texture {100} + {111} and {210} + {111} with a grain size of 10–200 μm (Fig. 2(d)).

4. EXPERIMENTAL METHODS

At the Analysis and Testing Center, Northeastern University, the micro-morphological characteristics of nano-micron-sized spheroidal aggregates of FeS₂ were observed using an Ultra Plus Field Emission Scanning Electron Microscopy, and the distribution characteristics of colloidal pyrite components were analyzed using an Energy Dispersive Spectrometer (EDS).

At Institute of Mineral Resources, Chinese Academy of Geological Sciences, the major and trace element contents in nano-micron-sized spheroidal aggregates of FeS₂ contained in the ore were analyzed using a JXA-8230 electron microprobe. Test conditions: accelerating voltage: 20 kV, beam flux: 0.2 nA, beam spot: 5 μm .

At the Geological Laboratory, Central South University, a micro diffraction test on nano-micron-sized

spheroidal aggregates of FeS₂ was conducted using a D/Max Rapid IIR micro-XRD. Test conditions: CuK α ray ($\lambda = 0.154 \text{ nm}$); accelerating voltage: 40 kV, current: 250 mA, collimator diameter: 0.1 mm, exposure time: 20 min.

5. RESULTS

5.1. Microscopic Morphology of Spheroidal Aggregates of FeS₂

The spheroidal aggregates of FeS are mainly distributed at the edge of pyrrhotite or arsenopyrite, appearing as balls or spheroids in the optic microscope (Figs. 3(a–b)). There is cement filled among spheroidal aggregates. Parts of pyrite crystallized in early stages form into spheroids encapsulated by girdles outside (Figs. 3(a–c)). It can be observed that spheroidal aggregates of FeS₂ have been metasomatized or penetrated by arsenopyrite (Figs. 3(c–d)), and that spheroidal aggregates of FeS₂ are metasomatized and corroded by mineralized hydrothermal fluid formed later, resulting in fragmentary morphology of aggregates (Figs. 3(b–d)).

FE-SEM was used to observe the internal characteristics of spheroidal aggregates of FeS₂ (Fig. 4). It is observable that the first-generation pyrite (Py I) is encapsulated by spheroidal aggregates of FeS₂, and the contact boundary between them is evident (Fig. 4(b)); nano-sized

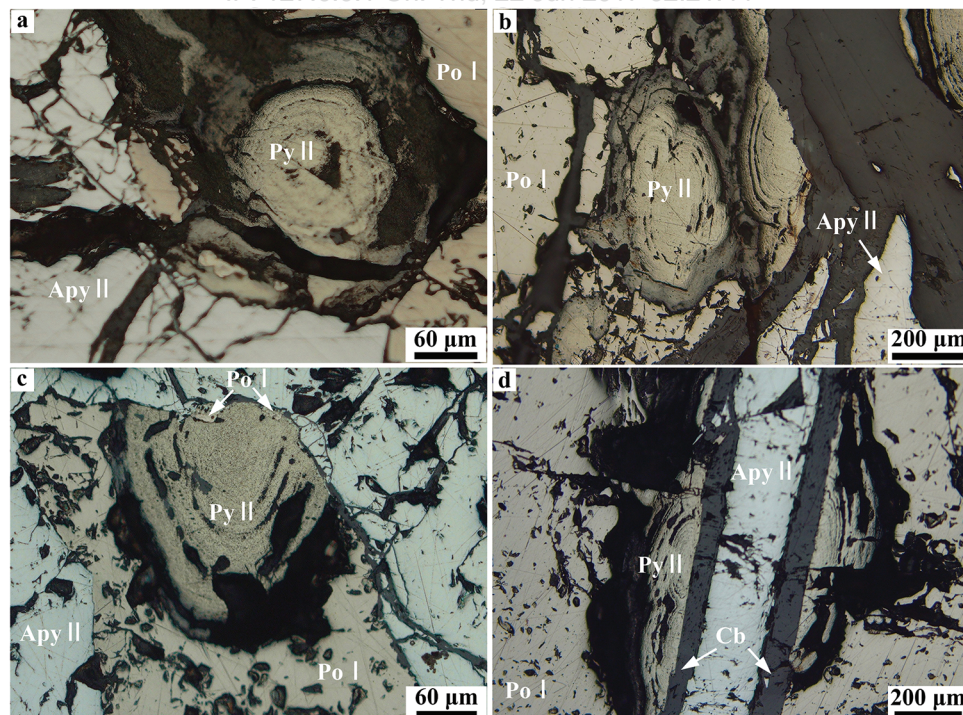


Figure 3. Different morphological characteristics of spheroidal aggregates of FeS₂ shown under microscope. (a) Spheroidal aggregates of FeS₂ are distributed at the edge of pyrrhotite; (b) Several spheroidal aggregates of FeS₂ are distributed as colloidal crystals at the edge of pyrrhotite (Po I), and modified by fluid later; (c) Spheroidal aggregates of FeS₂ are metasomatized by arsenopyrite, so residual crystals of pyrrhotite (Po I) are observable on the contact zone; (d) Spheroidal aggregates of FeS₂ are penetrated by arsenopyrite (Apy II), and fissures are filled by carbonate minerals; PyII-spheroidal aggregates of FeS₂, Po I-first-generation pyrrhotite; Apy II-second-generation arsenopyrite; Cb-carbonate minerals.

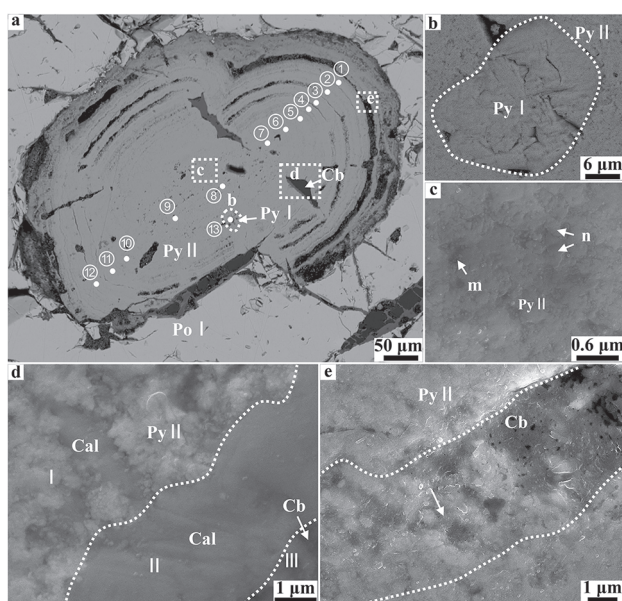


Figure 4. Microscopic morphological characteristics of spheroidal aggregates of FeS₂. (a) Morphological characteristics of Py I and PyII; (b) Relatively euhedral pyrite (Py I) encapsulated in spheroidal aggregates of FeS₂, 6000 \times ; (c) Nanocrystalline grains with different levels of crystallization inside spheroidal aggregates of FeS₂, 50000 \times ; (d) Phase belt classification for carbonate minerals around the fissure of spheroidal aggregates of FeS₂, 30000 \times ; (e) Morphology of spheroidal aggregates of FeS₂ at the transition zone, 2000 \times . Py I-first-generation pyrite, Py II-spheroidal aggregates of FeS₂; Po I-first-generation pyrrhotite; Cal-calcite; Cb-carbonate minerals; m-nanocrystalline grain; n-euhedral crystalline grain.

crystalline grains of pyrite, part of which are euhedral, are aggregated and form the kernel of spheroidal aggregates of FeS₂, with a crystalline grain size of 50–300 nm (Area *n* in Fig. 4(c)); around the fissure of spheroidal aggregates of FeS₂ (Fig. 4(d)), there are three phase belts, namely, the FeS₂ nanocrystal accumulation zone (I), clacite (II) and carbonate minerals (III) from left to right, which are classified according to their phase characteristics, and the contact boundary is evident without metasomatism. No clear crystal shape can be found from the crystalline grains inside the FeS₂ nanocrystal accumulation zone (Fig. 4(d)); crystallized grains are visible at the transition zone between two girdles with a grain size <1 μ m, and on both sides of the transition belt, crystalline grains have different levels of crystallization and are cemented by carbonate minerals (Fig. 4(e)).

Spheroidal aggregates of FeS₂ have a zonal edge (Fig. 5(a)). For spheroidal aggregates of FeS₂ as shown in Area *E* of Figure 5(a), the boundary between the transition zone and the girdle is evident, and the crystalline grain size decreases gradually from the nanocrystalline grain accumulation zone to the transition zone, which is filled incompletely (Area *H* in Fig. 5(b)); at Area *F* in Figure 5(b), part of grains are in the form of euhedral crystals after crystallization (Area *n* in Fig. 5(c)).

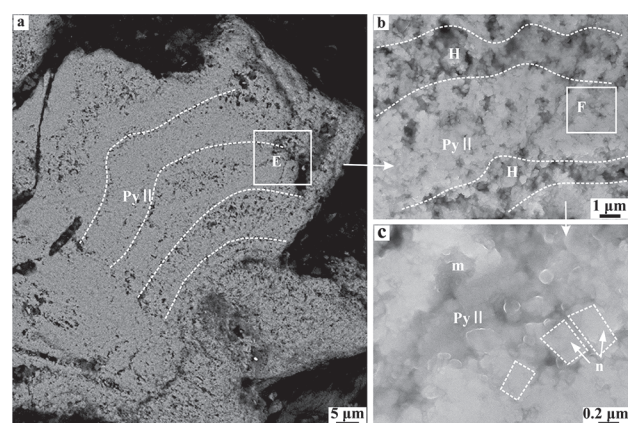


Figure 5. Morphological characteristics of spheroidal aggregates of FeS₂. (a) Zonal edge of spheroidal aggregates of FeS₂; (b) Morphological characteristics of spheroidal aggregates of FeS₂ at the transition zone; (c) FeS₂ nanocrystalline grains with different levels of crystallization; Py II-spheroidal aggregates of FeS₂; H-transition zone; m-nanocrystalline grains; n-euhedral crystalline grains.

The above results show that the cementation indicated as above is the result of aggregation and growth of nano-micron-sized FeS₂ crystalline grains; the density of nanocrystalline grains is uneven; there are unfilled areas on the transition zone between girdles, and grains have different levels of crystallization.

5.2. Component Analysis

Spheroidal aggregates of FeS₂ are determined for their components using an electron microprobe, as shown in Figures 4(a)(①–⑬). The results are as shown in Table I, which shows that the contents of Fe and S are 45.48–46.65 wt%, 50.86–53.28 wt% respectively, 45.84 wt% and 52.91 wt% on average, falling within FeS₂ series; in the kernel of spheroidal aggregates of FeS₂, the content of As is relatively low but remarkably high at the edge; the contents of Ni and Pb in spheroidal aggregates of FeS₂ is lower than the detection limit; the distribution of Co and Cu is irregular; Au is mainly distributed in the kernel of spheroidal aggregates of FeS₂, with a low content ranging from 0.01 wt% to 0.05 wt%.

See Figure 6 for the distribution testing on elements as shown in Figure 4(a). The test is targeted to two elements, namely, Fe and S. Test shows that the intensity of S weakens at the edge of spheroidal aggregates of FeS₂, and the content of Fe is comparatively even (Figs. 6(b–c)); the distribution of Co is irregular (Fig. 6(d)), C, O and Si are similarly distributed, mainly at the fissure or edge of spheroidal aggregates of FeS₂ (Figs. 6(e, f and i)); Ca and Sb are similarly distributed, mainly in carbonates (Figs. 6(g–h)).

The results show that Fe and S are two major elements in spheroidal aggregates of FeS₂; at the edge or inside the fissure of spheroidal aggregates of FeS₂, low temperature minerals such as carbonates (e.g., calcite and siderite) or chalcedony dominate.

Table I. Electron microprobe analysis of spheroidal aggregates of FeS₂ (wt%).

Sample no.	Positions	S	Fe	Co	Cu	Zn	Sb	As	Ag	Au	Ni	Pb	Total	Fe/S
1	Exterior zone	50.86	45.64	0.04	0.01	0.05	0.01	0.07	0.01	<mdl	<mdl	<mdl	96.69	0.52
2	The band 3	52.98	45.61	0.08	0.05	<mdl	0.06	0.01	<mdl	<mdl	<mdl	<mdl	98.79	0.49
3	The band 2	53.11	45.48	0.11	0.01	<mdl	<mdl	<mdl	<mdl	<mdl	<mdl	0.01	98.72	0.49
4	The band 1	52.23	46.03	0.03	<mdl	0.01	0.01	0.02	<mdl	<mdl	<mdl	<mdl	98.33	0.51
5	The kernel	52.90	46.65	0.09	<mdl	0.07	0.01	0.04	0.01	0.01	<mdl	<mdl	99.78	0.51
6	The kernel	53.19	45.8	0.05	0.01	0.08	<mdl	0.04	<mdl	<mdl	<mdl	<mdl	99.17	0.49
13	The kernel	53.09	45.86	0.07	0.20	0.14	<mdl	0.20	<mdl	0.01	<mdl	0.01	99.58	0.50
7	The kernel	53.28	46.20	0.07	0.06	<mdl	0.09	0.04	<mdl	0.03	<mdl	<mdl	99.77	0.50
8	The kernel	52.95	46.14	0.04	0.01	0.03	0.06	0.02	0.01	0.04	<mdl	<mdl	99.30	0.50
9	The kernel	52.95	45.55	0.09	0.03	0.02	0.07	0.08	0.02	0.03	<mdl	<mdl	98.84	0.49
10	The band 1	53.21	45.75	0.06	0.01	0.03	0.01	0.06	0.01	<mdl	0.02	<mdl	99.16	0.49
11	The band 2	53.21	45.92	0.07	0.02	<mdl	<mdl	0.04	0.01	<mdl	<mdl	<mdl	99.27	0.50
12	Exterior zone	52.82	46.24	0.08	0.01	0.05	0.03	0.08	<mdl	0.05	<mdl	<mdl	99.36	0.50

Note: <mdl = below minimum detection limit.

5.3. Mineral Characteristics

A determination was conducted on the structure of crystals at Points b, c and d, and the result is as shown in Figure 7.

The crystal face diffraction peaks of pyrrhotite (200), (203), (206) and (220), mainly composed of monocline pyrrhotite (Fe₇S₈) (Point b in Fig. 7), are remarkably sharp. The main phases in spheroidal aggregates of FeS₂ are pyrite + marcasite (Figs. 7(c–d)). As viewed from the

intensity of diffraction peaks, the crystal face diffraction intensity of pyrite (200) and (311) in the center is remarkably higher than that at the edge; the crystal face diffraction intensity of marcasite (110) and (120) is lower than that at the external girdles. The results show that at the spheroidal aggregates of FeS₂, pyrite enjoys a good crystallization in the center, accompanied by less marcasite; marcasite at the edge enjoys a better crystallization

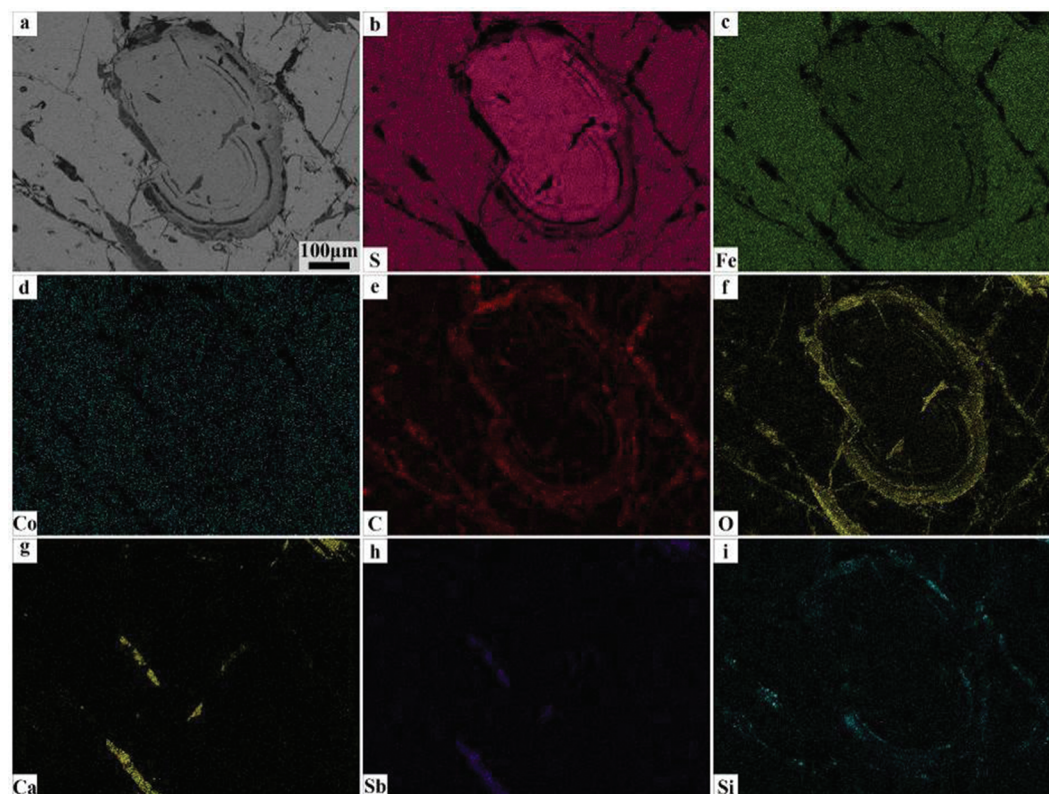


Figure 6. Trace elements and backscattered electron images of spheroidal aggregates of FeS₂ from the Laozuoshan gold deposit. (a) Backscattered electron images of the test area; (b) Intensity of S weakens at the edge of spheroidal aggregates of FeS₂; (c) Fe is distributed evenly in spheroidal aggregates of FeS₂; (d) The distribution of Co is irregular; (e) C is mainly distributed at the edge or in the fissure of spheroidal aggregates of FeS₂; (f) O is mainly distributed at the edge or in the fissure of spheroidal aggregates of FeS₂; (g) Ca is mainly distributed at the edge or in the fissure of spheroidal aggregates of FeS₂; (i) Si is mainly distributed at the edge of spheroidal aggregates of FeS₂.

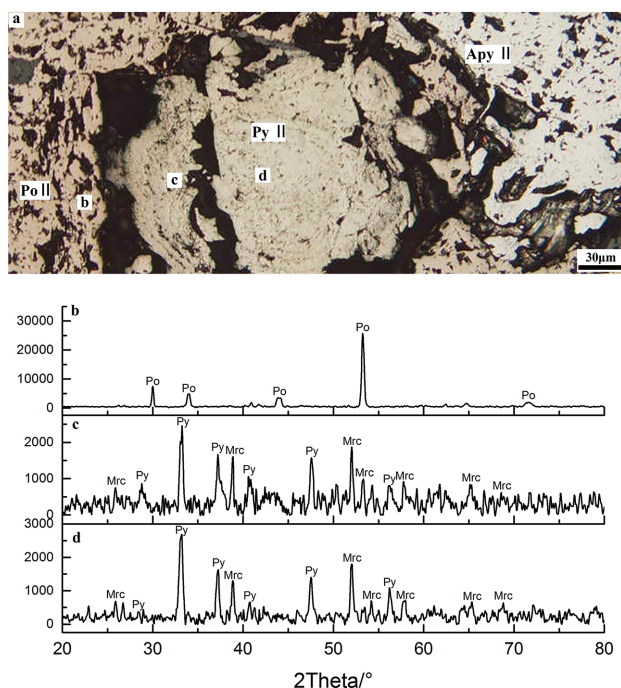


Figure 7. *In situ* micro-XRD data graph. (a) The test area images of spheroidal aggregates of FeS₂; (b) The diffraction diagram of pyrrhotite; (c) The diffraction diagram of spheroidal aggregates of FeS₂ at the edge; (d) The diffraction diagram of spheroidal aggregates of FeS₂ kernel; Po-Pyrrhotite; Py-Pyrite; Mrc-Marcasite.

condition, so marcasite dominates in the crystallization products, accompanied by less pyrite.

6. DISCUSSION

6.1. Physicochemical Conditions for Mineralization

Temperature measurement for the fluid inclusion inside the skarn mineralization zone of the Laozuoshan gold deposit shows that the mineralization temperature ranges from 237.7 °C–480 °C.³⁸ The metal sulfide fluid inclusions formed during the early and late mineralization periods are mainly composed of CO₂, H₂O, CO, CH₄, N₂, Na⁺, NO₃⁻, Cl⁻ and SO₄²⁻, etc. This research area is formed mainly from skarn by means of its mineralization, and during the skarn mineralization periods, the pH value of fluid ranges from 4.37 to 6.82, the Eh value ranges from -0.5 to -0.32, which imply a low-salinity, weak-acidity and weak-reducibility mineralization condition.³⁸ The stable isotope geochemical test analysis shows the ore-forming hydrothermal fluid from the Laozuoshan gold deposit is mainly composed of magmatic water, possibly intermingled with a small amount of surface water, and the ore-forming matters mainly come from the mantle or upper crust of the earth.⁴⁰

As a product of the late skarn mineralization period, spheroidal aggregates of FeS₂ are generated from the tectonic contact zone between migmatitic granite and skarn, which is closely associated with the physicochemical conditions for their formation. Once formed, part of

spheroidal aggregates of FeS₂ are solved in fluid and further metasomatized by fluid under the hydrothermal action happened later. It follows that the physicochemical environment of the mining area serves as basic conditions for the formation of spheroidal aggregates of FeS₂.

6.2. The Formation of Spheroidal Aggregates of FeS₂

Based on the crystal nucleation theory, we can obtain a formula about spherical crystal nucleus as below:⁴¹

$$\Delta G = -\frac{4}{V}\pi r^3 k_B T \ln(S) + 4\pi r^2 \gamma \quad (1)$$

In formula (1), where G represents the total free energy of the new interface and new volume produced when a new phase is being formed, V represents the volume of atomic groups, r represents the radius of crystal nucleus, k_B represents Boltzmann constant, S represents saturation, γ represents the surface free energy per unit area. As can be obtained from Formula (1), when $S > 1$, ΔG has a positive limit value at r^* , the nucleation radius of crystal nucleus, which is decided by $d\Delta G/dr = 0$. When S is a fixed value, all atomic groups that meet $r > r^*$ grows into stable crystal nuclei with the decline in their free energy, while crystal nuclei will be solved when $r < r^*$.

$$r^* = \frac{2V\gamma}{3k_B T \ln(s)} \quad (2)$$

As can be seen from Formula (2), nucleation can be accelerated by increasing the saturation of solution to drop the nucleation radius r^* . Impurities or seed crystals in the metastable fluid can effectively drop the surface potential barrier during nucleation; under the conditions of lower super-saturation and super-cooling, heterogeneous nucleation happens first on the surface of impurities or seed crystals.⁴² Due to insufficient crystallization of foreign matters or seed crystals caused by their nucleation in heaps in a short time, nano-sized crystals are common. In general, nano-sized crystals have high-index crystal surface, higher surface free energy and larger specific surface area. In the process of aggregation and growth, nano-sized crystal grains become easier to aggregate with each other under the hydrothermal drive.⁴³

Spheroidal aggregates of FeS₂ in this mining area are mainly aggregates of nano-micron-sized pyrite and marcasite, of which the nano-sized crystalline grains appear as microspherulitic aggregates, and euhedral crystalline grains are visible occasionally. Analysis suggests that in the middle and late skarnization periods, the concentration of ions in fluid increases and the change in fluid environment leads to a rise in the super-saturation or super-cooling of fluid, in this case, Fe reacts with S to produce nano-micron-sized FeS₂ crystalline grains. Following the formation of crystal nucleus, a crystal-medium interface takes shape. The interface status (interface roughness, growth driving force, and interface stability) has a direct effect on the crystal growth process; during which part of the grains develop into euhedral crystalline grains gradually.⁴²

6.3. Mechanism on the Formation of Spheroidal Aggregates of FeS₂

Generally, skarn deposits may experience steam-water hydrothermal metasomatism several times before formation. In these courses, there is a great change in the physicochemical conditions for rock or ore forming, which leads to continuous evolution and alteration of metasomated minerals.^{44,45} In the process of skarn deterioration, during which the temperature of hydrothermal events goes down, skarn minerals are formed at the early stage of metasomatism and low-salinity fluid formed later may reach its steam pressure curve only when boiling happens for the first time. Therefore, sulfide minerals are what are mainly released at the deterioration stage.^{46,47}

In previous researches, the nano-sized grains of FeS₂ grow in two ways: generally in the sedimentation environment, nano-sized grains of FeS₂ aggregate and form framboidal pyrite, and the spherical micro crystals formed grow further to form euhedral pyrite, as indicated in Figure 8-pathway A;⁴⁸⁻⁵⁰ or nano-sized grains of FeS₂ accumulate continuously to form a kernel, which grows along its radius directions to form a girdle. When the grain size of crystals outside the girdle increases and becomes too large, the interface location between crystal grains starts to be adjusted to form crystals with a certain crystallization direction gradually so as to achieve

the lowest state of energy as a whole, as indicated in Figure 7-pathway B.¹⁶

Nano-micron-sized spheroidal aggregates of FeS₂ sampled from Laozuoshan are closely correlated with monocline pyrrhotite and arsenopyrite, with a multi-girdle structure, which is composed of nano-sized pyrite and marcasite, but their characteristics and growth means are different from colloidal and framboidal pyrite.

Based on the characteristics of Laozuoshan skarnization and the physicochemical conditions of this area, analysis suggests that at the sulfide mineralization stage of the skarn mineralization periods, scattered grains in nano size, which are located in a static fluid environment, enjoy higher surface energy and are easy to aggregate together; part of nano-sized grains of FeS₂ are crystallized from fluid, due to uneven distribution of pyrite (Py I) crystallized in the early stage, adhere around the first-generation pyrite and aggregate into kernels under the drive of surface energy, as indicated in Figure 8-pathway C; the other part of nano-sized grains of FeS₂ aggregate together to form kernels with the aid of free energy between crystal grains, as indicated in Figure 8-pathway D. During the aggregation of microcrystals, a single microcrystal or the whole aggregate tends to appear as a sphere so that they have the lowest surface energy.¹⁹ With the changes in physicochemical conditions (Eh, pH or temperature) of fluid and

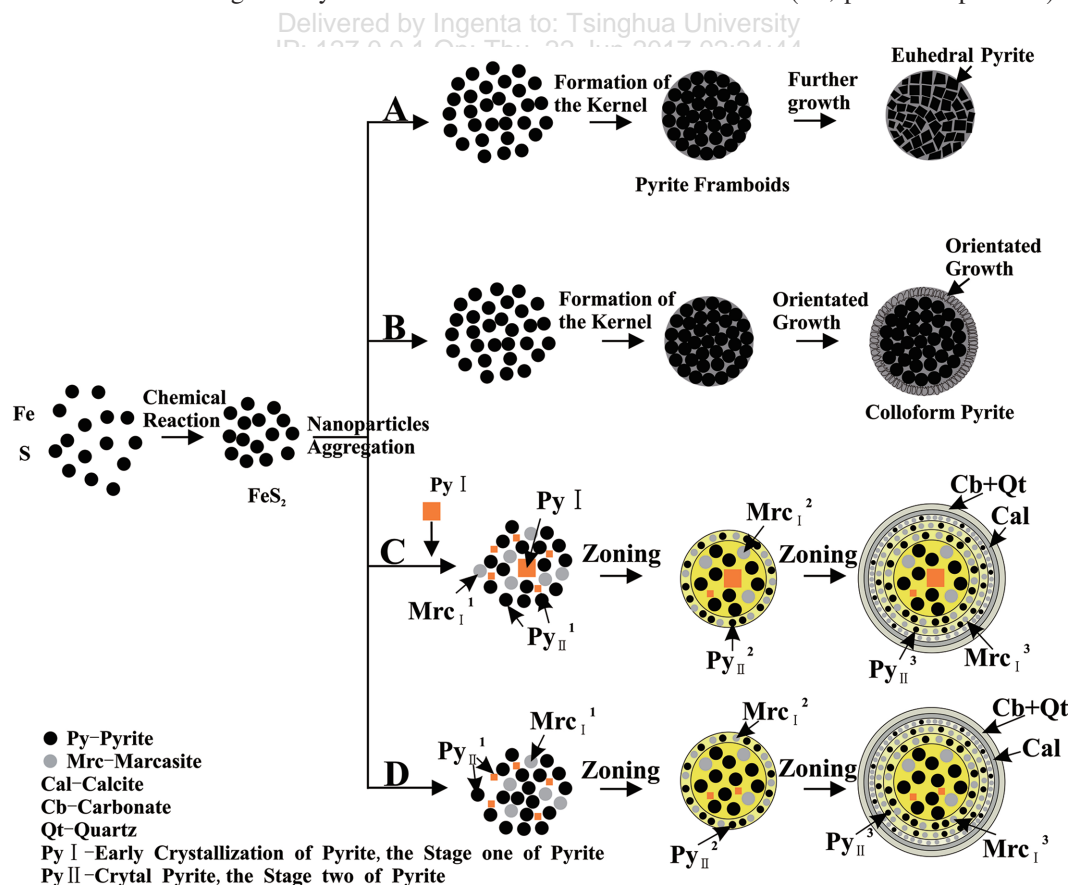


Figure 8. Growth pattern and formation mechanism diagram for nanocrystalline pyrite.

xenomorphic crystals, with a grain size of 50 nm–1 μm. The components of the spheroids are relatively stable, but a loss in S appears at the edge of the spheroids, where the content of As increases significantly.

(3) The characteristics of spheroidal aggregates of FeS₂ sampled from Laozuoshan reflects that during the skarnization process of this mining area, the ore forming fluid experienced a transition from high temperature, medium acidity to low temperature, weak acidity; the fluid is relatively stable, with a relatively high super-saturation and lower temperature.

Acknowledgments: We acknowledge the financial support from the National Natural Science Foundation of China (Grant No. 41272062), and the Open Fund of State Key Laboratory of Ore Deposit Geochemistry (Institute of Geochemistry, Chinese Academy of Sciences, Guiyang) (Grant No. 201308). Authors would like to thank Lixin Yin and Huili Li (Northeastern University) for their help in FE-SEM(EDS) and thank Dr. Zhenyu Chen (the Chinese Academy of Geological Sciences) for their support in the electronic probe micro-analyzer. Thanks to Xiangping Gu (Central South University) for help *in situ* micro X-ray diffractions.

References and Notes

- J. B. Murowchick and H. L. Barnes, *American Mineralogist* 72, 1241 (1987).
- G. Y. Chen, D. S. Sun, L. Zhang, W. S. Zang, J. Wang, and A. H. Lu, *Geoscience* 1, 60 (1987).
- F. Huang, N. C. Wang, W. L. Zhang, Y. Z. Yao, Y. D. Peng, and D. M. Kou, *Chinese Science Bulletin* 54, 4479 (2009).
- L. Wang and Y. F. Zhu, *Ore Geology Reviews* 69, 243 (2015).
- J. B. Murowchick, *Economic Geology* 87, 1141 (1992).
- M. A. A. Schoonen and H. L. Barnes, *Geochimica et Cosmochimica Acta* 55, 1495 (1991).
- M. A. A. Schoonen and H. L. Barnes, *Geochimica et Cosmochimica Acta* 55, 1505 (1991).
- J. H. Chen, G. F. Ge, and J. R. Wang, *Mineral Deposits* 26, 643 (2007).
- J. R. Craig, *the Canadian Mineralogist* 39, 937 (2001).
- W. M. Peace, M. W. Wallace, M. P. Holdstock, and J. H. Ashton, *Mineralium Deposita* 38, 568 (2003).
- J. J. Wilkinson, S. L. Eyre, and A. J. Boyce, *Economic Geology* 100, 63 (2005).
- A. Pacevski, R. Moritz, K. Kouzmanov, K. Marquardt, P. Zivkovic, and L. Cvetkovic, *The Canadian Mineralogist* 50, 1 (2012).
- H. Ohfuji, A. P. Boyle, D. J. Prior, and D. Rickard, *American Mineralogist* 90, 1693 (2005).
- H. Ohfuji, D. Rickard, M. E. Light, and M. B. Hursthouse, *Eur. J. Mineral* 18, 93 (2006).
- K. Fretag, A. P. Boyle, E. Nelson, M. Hitzman, J. Churchill, and M. Lopez-Pedrosa, *Mineralium Deposita* 39, 103 (2004).
- C. D. Barrie, A. J. Boyce, A. P. Boyle, P. J. Williams, K. Blake, T. Ogawara, J. Akai, and D. J. Prior, *American Mineralogist* 94, 415 (2009).
- A. F. Rogers, *J. Geology* 25, 515 (1917).
- D. F. Yang, D. X. Fu, and L. X. Wu, *Bull. Nanjing Inst. Geol. M. R., Chinese Acad. Geol. Sci.* 3, 59 (1982).
- S. Gao, F. Huang, X. P. Gu, X. Y. Li, L. Meng, R. Liu, L. Sun, W. Y. Gao, and H. T. Yu, *ACTA Geologica Sina (English Edition)* 88, 1770 (2014).
- B. M. England and J. Ostwald, *Ore Geology Reviews* 7, 381 (1993).
- Y. M. Pan and P. Dong, *Ore Geology Reviews* 15, 177 (1999).
- Y. S. Ren and L. D. Liu, *Mineral Deposits* 25, 95 (2006).
- Y. Zhang, Y. J. Shao, X. Zhou, Z. F. Liu, and M. H. Zheng, *The Chinese Journal of Nonferrous Metals* 23, 3492 (2013).
- R. E. Sweeney and I. R. Kaplan, *Economic Geology* 68, 618 (1973).
- F. Y. Chu and L. R. Chen, *Oceanologia et Limnologia Sinica* 26, 315 (1995).
- T. F. Zhou, L. J. Zhang, F. Yuan, Y. Fan, and D. R. Cooke, *Earth Science Frontiers* 17, 306 (2010).
- M. A. A. Schoonen, *Geological Society of America* 379, 177 (2004).
- Q. Q. Xie, T. H. Chen, Z. L. Fan, X. C. Xu, Y. F. Zhou, W. B. Shi, and J. J. Xie, *Scientia Sinica Terrae* 44, 2665 (2014).
- R. T. Wilkin, H. L. Barnes, and S. L. Brantley, *Geochimica et Cosmochimica Acta* 60, 3897 (1996).
- B. Marshall and L. B. Gilligan, *Ore Geology Reviews* 2, 87, (1987).
- D. Brown, *Mineral Deposita* 29, 330 (1994).
- N. Foley, R. A. Ayuso, and R. Seal, II., *Economic Geology* 96, 891 (2001).
- R. H. Bailie and D. L. Reid, *South Africa of Geological Society* 108, 51 (2005).
- R. A. Berner, *Geochimica et Cosmochimica Acta* 48, 605 (1984).
- M. F. Li, S. Q. Ye, Y. C. Yang, G. B. Zhang, X. G. Hou, T. X. Ming, and Z. Tang, *Global Geology* 33, 543 (2014).
- X. M. Li, X. W. Zhou, and X. Z. Li, *J. Mineral Petrol* 22, 25 (2002).
- B. L. He, *Gold* 23, 7 (2002).
- A. S. Zhao, Y. Wang, and W. G. Lu, *Gold* 25, 20 (2004).
- Z. X. Pei, B. L. He, Z. L. Han, and G. W. Ao, *Gold Geology* 10, 28 (2004).
- H. J. Zhang, *Gold* 20, 4 (1999).
- Y. Feng, T. Y. Ma, L. Liu, and Z. Y. Yuan, *Scientia Sinica Chimica* 39, 864 (2009).
- E. W. Shi, C. T. Xia, B. G. Wang, W. J. Li, R. L. Yuan, and W. Z. Zhong, *Science in China (Series E)* 27, 126 (1997).
- L. Z. Yao, Science and Technology of China Press (1995), Chap. 6, p. 258.
- Y. M. Zhao, Geology Publishing House (2012), Chap. 20, p. 339.
- T. A. O. Kwak, *J. Metamorphic Geol.* 4, 363 (1986).
- L. D. Meinert, *Geoscience Canada* 19, 145 (1992).
- L. D. Meinert, J. W. Hedenquist, H. Satoh, and Y. Matsuhisa, *Economic Geology* 96, 147 (2005).
- R. T. Wilkin and H. L. Barnes, *Geochimica et Cosmochimica Acta* 61, 323 (1997).
- X. Y. Yang and Y. M. Gong, *Earth Science-Journal of China University of Geosciences* 36, 643 (2011).
- Z. Sawlowicz, *Geol Rundsch* 82, 148 (1993).
- F. Huang, S. Gao, J. Liu, W. Y. Gao, H. Sun, Y. H. Wang, Y. D. Peng, and Y. Z. Yao, *Earth Science Frontiers (China University of Geosciences(Beijing); Peking University)* 20, 110 (2013).
- Q. J. He, *J. CSIMM* 1, 54 (1984).

Received: 2 March 2016. Accepted: 2 October 2016.